

Delbrück and nuclear Raman scattering of 10.83-MeV photons by deformed and spherical heavy nuclei*

H. E. Jackson and G. E. Thomas

Argonne National Laboratory, Argonne, Illinois 60439

K. J. Wetzel

University of Portland, Portland, Oregon 97203

(Received 12 November 1973)

A beam of monoenergetic γ rays, extracted from the CP-5 reactor, has been used in a high-resolution measurement of the differential cross sections for photon scattering by Tb, Ta, Pb, Bi, Th, and ^{238}U . The spectrum of scattered photons was observed with a resolution of ~ 10 keV in a Ge(Li) detector whose sensitive volume was ~ 60 cm³. For Pb and U extensive measurements of the angular distributions for elastic and inelastic scattering were measured. For scattering angles $\theta < 45^\circ$ the elastic scattering is dominated by the Delbrück effect. With the possible exception of Ta, for $\theta > 90^\circ$ (where only nuclear resonance and Thomson scattering are important) both the magnitude and angular dependence of the elastic scattering cross section are in good agreement with the values which follow from the most recent photoabsorption cross sections in the corresponding targets. To an accuracy of $\sim 10\%$ the elastic and inelastic (nuclear Raman) scattering for U and Th can be deduced from the simple rotator model using the parameters implied by the photoabsorption data. A trend of Raman scattering to be 10% weaker than expected is suggested by the data. For Ta and Tb the Raman scattering is substantially weaker than expected.

NUCLEAR REACTIONS ^{159}Tb , ^{181}Ta , Pb, ^{209}Bi , ^{232}Th , $^{238}\text{U}(\gamma, \gamma')$, $E_\gamma = 10.83$ MeV; measured $\sigma(\theta)$, elastic scattering, inelastic scattering to g.s. rotational band. Ge(Li) detector, 10 keV at 10 MeV.
--

I. INTRODUCTION

The study of elastic and inelastic scattering of 1–10-MeV photons by heavy nuclei can be of great value in understanding both fundamental interactions such as Delbrück scattering¹ and details of the giant dipole resonance—especially if the measurements can be performed with sufficient precision and energy resolution to separate elastic and inelastic scattering. The elastic scattering arises from two types of processes: scattering by the nucleus considered as a point charge, i.e., nuclear Thomson, and Coulomb elastic or Delbrück scattering; and scattering arising from the internal structure of the nucleus; for example, nuclear resonance scattering. Nuclear Thomson scattering is a classical effect, Delbrück scattering is predicted by quantum electrodynamics as a radiative correction to nuclear Thomson scattering, and nuclear resonance scattering is described by photonuclear reaction theory. Because these reactions are indistinguishable, each contributes coherently to the total elastic scattering amplitude. To the extent that nuclear resonance scattering is assumed to proceed through an

intermediate state such as the giant dipole resonance, inelastic scattering can also occur. Such scattering, commonly referred to as nuclear Raman scattering,^{2,3} arises because the intermediate state can decay by photon emission to low-lying excited states as well as to the ground state of the target nucleus. The Delbrück effect, elastic scattering of photons by an electric field, continues to be of interest as a fundamental process, while nuclear Raman scattering is important because of its relationship to the photonuclear interaction in the energy region of the giant dipole resonance.

Until recently, attempts to measure the Delbrück effect⁴ have been unsuccessful for one of several reasons. In addition to contributions from the nuclear processes mentioned above, elastic scattering can include a coherent contribution from atomic Rayleigh scattering. At photon energies of ≤ 2.6 MeV, where monochromatic photons are readily obtained from radioactive sources, Rayleigh scattering competes strongly with Delbrück scattering; because the Delbrück and Rayleigh scattering cross sections are both sharply peaked in the forward direction they cannot be

experimentally distinguished by their angular variation dependence. Measurements at higher energies, until a few years ago, involved the use of scintillation crystals for detection of the scattering photon. In these experiments the energy resolution did not permit the separation of the elastic from the inelastic scattering events. Other experimental problems existed at higher photon energies ($E_\gamma > 15$ MeV) where Rayleigh scattering could be neglected; photons were produced either by Bremsstrahlung techniques, thus preventing a precise energy definition, or by nuclear particle reaction such as ${}^7\text{Li}(p, \gamma)$ for which the photon intensity was limited. The most convincing evidence of the Delbrück effect prior to the advancement of the high-resolution Ge(Li) spectrometers is that of the Zürich group of Bösch *et al.*⁵ who scattered monochromatic 9-MeV photons from lead and uranium targets. The forward peaking expected for the Delbrück effect was observed in the scattering cross section although the elastic and inelastic scattering were not experimentally resolved; the inclusion of an estimated Delbrück amplitude gave a reasonably good agreement between the predicted cross section and the observed forward-angle data. The experimental results for uranium at large scattering angles ($\theta > 60^\circ$) were observed to be higher than predicted. Recent results have shown that this discrepancy in the elastic scattering results is due to the presence of a strong unresolved Raman inelastic line at these angles. Unambiguous observation of the Delbrück effect using a Ge(Li) detector to precisely identify the elastic scattering events have been reported recently by the present authors⁶ and by Moreh, Salzman, and Ben-David⁷ who observed the scattering of 10.83- and 9.0-MeV photons, respectively, from high- Z targets. In both measurements monochromatic photons were produced in neutron-capture reactions. The insignificant contribution of Rayleigh scattering at these photon energies and scattering angles ($\theta > 20^\circ$) simplifies the interpretation of the experimental results. The very large elastic scattering cross sections at the forward angles can be interpreted only as Delbrück scattering. Several high-resolution measurements⁸⁻¹⁰ of elastic scattering of 1.33-MeV photons from lead and uranium also have been reported recently. At this energy Rayleigh scattering dominates at the forward angles and the possible existence of a small Delbrück scattering amplitude is usually introduced to produce better agreement between calculated and measured cross sections. However, a lack of precise theoretical Rayleigh scattering amplitudes, particularly the size and relative phase of l -shell contributions make it vir-

tually impossible to establish the existence of Delbrück scattering from a low-energy measurement alone.

Experimental difficulties in measuring inelastic Raman scattering in the past were encountered in producing a monoenergetic photon beam and in measuring the scattered-photon energy spectrum with sufficient resolution to separate inelastic from elastic events—in medium and heavy-nuclei elastic and inelastic γ -ray groups may differ in energy by as little as 50 to 100 keV. The techniques of producing high-energy photon beams has been reviewed by Hayward.¹¹ Some of these techniques, for example the bremsstrahlung monochromator or positron annihilation in flight, can produce intense variable-energy photon beams in the range of 10 to 40 MeV but with a spread in energy of 100 to 500 keV which does not permit separation of elastic from inelastic scattering. The use of scintillation detectors with their limited resolution compounds this ambiguity. Because of these difficulties nearly all of the early studies of photon scattering focused on the study of “quasi-elastic” scattering, i.e., scattering in which photons which populate low-lying levels in the residual nucleus as well as the ground state are detected but are unresolved in energy. In 1962 Fuller and Hayward¹² reported the measurement of the cross section at 90° for scattering of bremsstrahlung-produced photons by the deformed nuclei ${}^{165}\text{Ho}$ and Er of natural isotopic abundance. The theoretical cross section for elastic scattering was smaller than the observed value; but they could be brought into agreement by assuming that an inelastically scattered γ ray was also detected along with photons from the elastic events. This was one of the earliest instances of an implicit nuclear Raman effect. The first reports of a high-resolution direct measurement of the inelastic component of scattering were made by the present authors¹³ and by Haas, Moreh, and Salzman.¹⁴ Both these experiments utilized reactor-produced photons and high-resolution Ge(Li) spectrometers. In these experiments energy differences of 45 keV between elastic and inelastic groups were readily resolved for thorium and uranium scatterers.

In this paper we wish to present the complete results of a program of high-resolution measurements of the scattering of 10.83-MeV photons by nuclei ranging from Tb to U.

II. EXPERIMENTAL DETAILS

The measurements were carried out in a highly collimated beam of capture γ rays obtained by irradiating one of two nitrogen-rich samples, either 350 g of melamine ($\text{C}_3\text{H}_6\text{N}_6$) or 170 g of

beryllium nitride (Be_3N_2), at the center of a tube which traverses the core of the Argonne CP-5 reactor. The 10.83-MeV γ ray is the ground-state transition in the reaction $^{14}\text{N}(n, \gamma_0)^{15}\text{N}$. The melamine and beryllium nitride contain 0.2 and 0.1 cm^2 , respectively, of nitrogen for production of the 10.83-MeV transition. The scattering targets were placed in the external photon beam at a point about 7 m from the center of the reactor; Fig. 1 shows the experimental arrangement. The scattering targets, metallic sheets about 1 cm thick and $5 \times 10 \text{ cm}$ in area, were placed on the beam axis and illuminated by a 3.8-cm-diam photon beam. By use of a small aperture (3-mm) collimator in front of the detector a scan of the beam profile established that the intensity was essentially uniform over the entire circular area. The scattering targets were aligned at a predetermined angle to give a reflection geometry for $\theta \geq 90^\circ$ and a transmission geometry for $\theta < 90^\circ$. The distance from target center to the detector cryostat was typically 11.5 cm, and the actual position of the detector within the cryostat was determined by using a radioactive source to measure an effective detector-source distance. The angular resolution of the detector used in the majority of the measurements was 5.3° . Detector position could be varied in angle between 20 and 150° relative to the incident beam direction. Limitations on this range of angles were imposed by detector housing, local shielding, and cryostat bulk.

The duration of runs for each target and angle were typically 3000–4000 min. The stabilized pulse-height analysis system eliminated observable drift or gain shift over these long times. Runs were normalized in terms of kWh of reactor operation to account for all variations both long

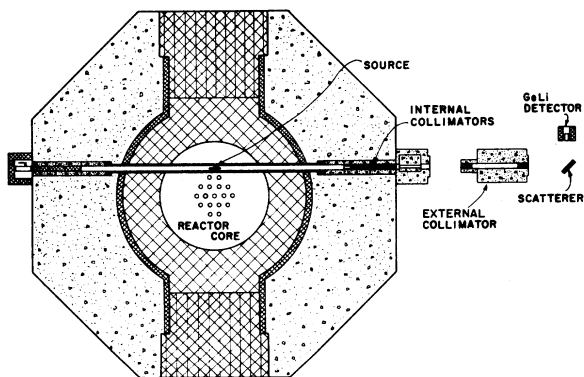


FIG. 1. Experimental arrangement at the Argonne CP-5 reactor showing the location of the internal target, the collimation system, scatterer, and detector. The melamine source can be replaced by a beryllium nitride source. Distance between the reactor center and the scatterer is about 7 m. Local shielding is not shown.

and short term in the incident photon intensity. Auxiliary experiments were performed to establish the reliability of the reactor power as a measure of the incident photon flux.

The high-energy portion of the spectrum of incident γ rays is shown in the lower part of Fig. 2. In this series of measurements the scattered radiation was detected in a Ge(Li) detector with approximately 60-cm^3 sensitive volume and an

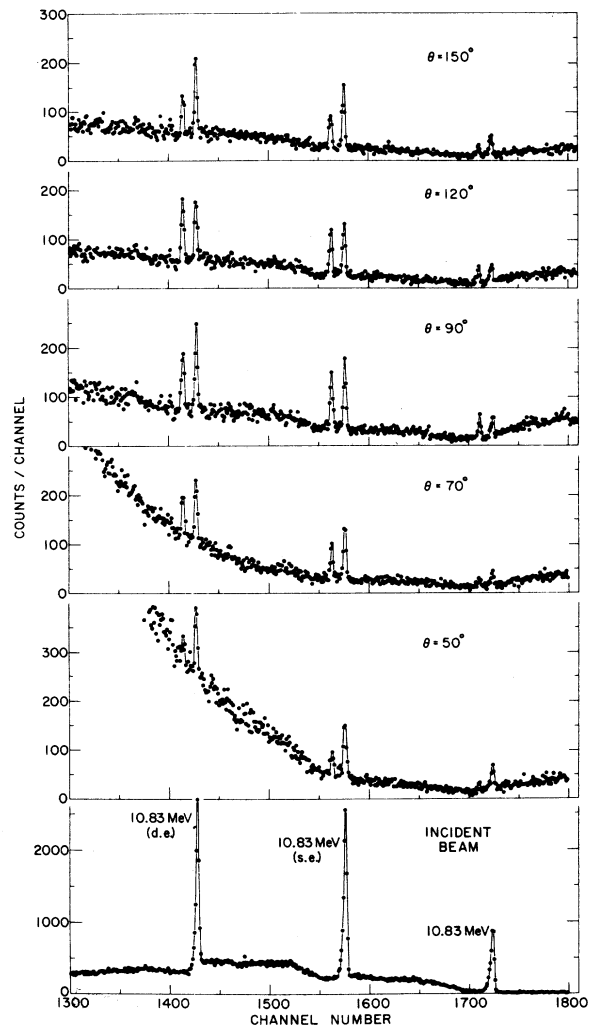


FIG. 2. High-energy portion of the spectra of 10.83-MeV radiation scattered from a U target at several angles and, at the bottom of the figure, a comparable spectrum of incident radiation. This shows the energy calibration of the detector-analyzer system as well as the detector response to 10.83-MeV photons, which is dominated by the double-(two annihilation photons) escape and single-(one annihilation photon) escape peaks. In the scattered spectrum at each angle, the 10.83-MeV photons from elastic scattering, and those of slightly lower energy from inelastic scattering to the 48-keV state, are clearly resolved.

energy resolution width, full width at half maximum, of 10 keV at 10 MeV. In the region of interest the single- and double-escape peaks dominate the detector response and only these were used in determining scattering cross sections. Although other discrete lines occur at somewhat lower energies (≤ 9.5 MeV) an increasingly high background prohibited the analysis of the spectra to determine scattering cross sections for these energies. The spectrum of scattered radiation was measured at a variety of scattering angles and for several targets. Figure 2 shows spectra taken at 30 to 150° for photons scattered from a uranium target 0.7 cm thick. When each series of measurements was begun or when any changes were made in the experimental setup, such as the collimation system, an additional measurement of the scattering by U at 90° was made as a reference spectrum. For each target and scattering angle analysis of the spectrum gave the cross section for elastic and for Raman scattering relative to that for scattering by uranium at 90°, as determined from the appropriate reference spectrum.

The absolute differential cross section for scattering at 90° (30° in the data reported in Ref. 6) by uranium was determined in a separate measurement using the same detector in sequence to measure the intensity of the 10.83-MeV line in the incident photon beam and in the scattered beam at 90°. Corrections for solid angle, detector efficiency, the small spatial variation in beam intensity, and absorption of photons were made in evaluating the absolute cross section. As previously mentioned the photon intensity profile of the incident beam was measured. Similarly, the entire detector face was scanned with a collimated 3-mm beam to determine the relative efficiency profile of the detector sensitive area; ~10% lower efficiency for photons incident on the detector center, explained by the intrinsic core region near the rear of the "five-sided" detector, was readily observed. The correction for a 15-cm lead absorber, used to attenuate the beam during the incident flux normalization, was measured directly rather than relying on theoretical absorption coefficients. Corrections were made in all cases for the effect of absorption of the incident and scattered photons in the target material itself and for the absorption of scattered photons in the detector germanium and detector cryostat window.

Of the two previous absolute measurements of $d\sigma/d\Omega$ for U, we now know the second to have been too large because of a background of 10.83-MeV photons which result when background neutrons are captured in the liquid nitrogen in the detector reservoir system. This systematic error ordi-

narily is very small; however, for this 90° measurement a narrow (1.27-cm-diam) external collimator was used to insure that only the central region of the detector was illuminated. In comparison to normal running conditions, for which a 2.54-cm collimator was inserted, this calibration run had a lower counting rate and the importance of the background was accentuated. In the earlier 30° measurement this background effect was not as important for two reasons: The scattering cross section is itself 5 times larger than at 90°; and the same large collimator was used for calibration and for runs. Both tend to diminish the role of the background which we confidently estimate, based on several internal checks and on measurements under similar conditions, to have been less than 0.02 mb/sr in the 30° measurement.

The analysis based on the 90° U result has been reevaluated using the inelastic line at 10.79 MeV in place of the elastic peak; the intensity of this

TABLE I. Differential cross sections measured for elastic and inelastic scattering of 10.83-MeV photons. State or states populated by inelastic scattering are indicated in parentheses below the target. The errors given result from the statistical error in the measurement of the cross section relative to the calibration value, the 90° uranium inelastic cross section.

Nucleus	θ (deg)	$d\sigma/d\omega$ (elastic) (mb/sr)	$d\sigma/d\omega$ (inelastic) (mb/sr)	
²³⁸ U (2 ⁺ , 45 keV)	20	1.72 ± 0.17		
	30	0.97 ± 0.12		
	50	0.334 ± 0.039		
	60	0.23 ± 0.04		
	70	0.245 ± 0.024	0.136 ± 0.015	
	90	0.182 ± 0.017	0.154 ± 0.012	
	120	0.189 ± 0.017	0.160 ± 0.013	
²³² Th (2 ⁺ , 45 keV)	150	0.303 ± 0.016	0.160 ± 0.015	
	90	0.129 ± 0.015	0.103 ± 0.007	
	Pb	20	1.28 ± 0.12	
		30	0.55 ± 0.07	
		50	0.289 ± 0.051	
		60	0.20 ± 0.04	
		70	0.087 ± 0.014	
90		0.079 ± 0.005		
²⁰⁹ Bi ($\frac{7}{2}^-$, 910 keV)	120	0.060 ± 0.004		
	150	0.127 ± 0.008		
²⁰⁹ Bi ($\frac{7}{2}^-$, 910 keV)	90	0.101 ± 0.0062	~0	
¹⁸¹ Ta ($\frac{9}{2}^+$, 136 keV)	90	0.0370 ± 0.003	0.00656 ± 0.0015	
¹⁵⁹ Tb ($\frac{5}{2}^+$, 58 keV)	90	0.0314 ± 0.003	0.0110 ± 0.0016	
	¹⁵⁹ Tb ($\frac{7}{2}^+$, 138 keV)		0.00511 ± 0.0011	

line is unaffected by the previously mentioned background of 10.83-MeV radiation. In addition, we have remeasured all relative scattering cross sections for scattering angles $\geq 90^\circ$ with liquid Ar_2 as the coolant in place of N_2 . The results for the relative strength of the elastic and inelastic lines in this last series of measurements is the same as the earlier measurements, indicating that the 10.83-MeV background was negligible in the earlier measurements of relative angular distributions.

The calibration value thus obtained for the standard absolute 90° U-differential-Raman cross section is 0.154 mb/sr shown in column 4 of Table I, the $\pm 8\%$ error in this number reflects the limited counting statistics of the 8000-min duration of the 90° measurement. The final results for the absolute differential elastic and inelastic scattering cross sections for the various targets and scattering angles are summarized in the same table. The 20° , 30° , and 60° results for lead and uranium are from the earlier reported results.

III. THEORY

The differential scattering cross section can be written as

$$\frac{d\sigma(\mathbf{E}, \theta)}{d\omega} = |\mathcal{R}|^2 = |a + ib|^2, \quad (1)$$

a and b being the real and imaginary parts, respectively, of the complex scattering amplitude. These amplitudes contain the energy dependence and angular variation of the scattering cross section, and are usually computed separately for the two polarization states of incident photons. For example, choosing a basis of $\tilde{\mathbf{e}}_{\parallel}$ and $\tilde{\mathbf{e}}_{\perp}$, the linear polarizations parallel and perpendicular to the scattering plane, requires a knowledge of the four reaction amplitudes a_{\parallel} , a_{\perp} , b_{\parallel} , and b_{\perp} . The basis vectors $\tilde{\mathbf{e}}'_{\parallel}$ and $\tilde{\mathbf{e}}'_{\perp}$ for the scattered photons describe a rotation of the initial basis vectors through an angle θ about a line normal to the scattering plane so that

$$\tilde{\mathbf{e}}_{\perp} \cdot \tilde{\mathbf{e}}'_{\perp} = 1, \quad (2a)$$

$$\tilde{\mathbf{e}}_{\parallel} \cdot \tilde{\mathbf{e}}'_{\parallel} = \cos \theta. \quad (2b)$$

For the processes of interest to us the amplitudes which describe scattering with spin-flip, i.e., polarization change, vanish. When the usual average over initial states and sum over final states is carried out, the scattering cross section for unpolarized incident radiation is

$$\frac{d\sigma}{d\omega} = |\mathcal{R}|^2 = \frac{1}{2} |a_{\parallel}|^2 + b_{\parallel}^2 + a_{\perp}^2 + b_{\perp}^2. \quad (3)$$

Each of the individual amplitudes of Eq. (3) includes contributions from each of the coherent processes, Thomson, Delbrück, nuclear resonance, and Rayleigh scattering. A simple and elegant method for computing scattering amplitude for any of these processes at the zero scattering angle is based on the optical theorem and the property of analytic continuation of the scattering amplitude as expressed in the Kramers-Krönig dispersion relations.¹⁵ The zero-degree amplitudes $a(E)$ and $b(E)$ are related by

$$a(E, \theta=0) = \frac{E}{\pi} \mathcal{P} \int_{-\infty}^{\infty} \frac{b(E', \theta=0) dE'}{E'(E-E')} \quad (4a)$$

and

$$b(E, \theta=0) = -\frac{E}{\pi} \mathcal{P} \int_{-\infty}^{\infty} \frac{a(E', \theta=0) dE'}{E'(E-E')}. \quad (4b)$$

Thus a knowledge of either a or b at zero degrees implies the existence of the other and further, if the functional form of, say, $b(E)$ is known, then $a(E)$ can be found at an arbitrary energy, hence at all energies, from Eq. (4a). In this form Eqs. (4a) and (4b) are of little use. However, the optical theorem relates the zero-angle imaginary scattering amplitude to the total cross section for that specific absorption process which is associated with the particular type of scattering

$$b(E, 0) = \frac{E}{4\pi\hbar c} \sigma^{\text{abs}}(E). \quad (5)$$

If the energy variation of $\sigma^{\text{abs}}(E)$ is known, for example from measurements, then $b(E)$ is determined for all energies and $a(E)$ may then be calculated from the dispersion relation (4a). The continuation of these amplitudes to other, nonzero scattering angles must be determined from other considerations. Using Eq. (5), Eq. (4a) may be rewritten

$$a(E, 0) - a(0, 0) = \frac{E}{2\pi^2\hbar c} \mathcal{P} \int_0^{\infty} \frac{E' \sigma^{\text{abs}}(E') dE'}{(E'^2 - E^2)}. \quad (6)$$

The several absorption processes and their corresponding higher-order scattering process which are related in this way are: pair production and Delbrück scattering, photonuclear absorption and nuclear resonance scattering, and photoelectric absorption and Rayleigh scattering. Strictly speaking, the dispersion relation in Eq. (6) accounts only for that part of the real scattering amplitude associated with the corresponding absorptive process. When $b(E')$ in Eq. (6) is determined by the nuclear photoabsorption cross section then the term $a(E, 0) - a(0, 0) \equiv a^{\kappa}$ gives the scattering amplitude associated only with nu-

clear resonance scattering through the giant-dipole state. The low-energy limit $a(0, 0)$ is non-zero here and is, in fact, the nuclear Thomson amplitude a^T so that

$$a(E, 0) = a^r + a^T \quad (7)$$

becomes the complete real nuclear scattering amplitude. In the discussion which follows the individual reaction amplitudes are discussed in more detail.

Nuclear Thomson scattering

The simplest of the scattering processes, nuclear Thomson scattering, arises from those interactions between the incident photon and the nucleus in which no internal nuclear states are excited. In this process the nucleus can be considered as a point charge, Ze of mass AM where A is the atomic number and M the nuclear mass. Just as for free electrons the low-energy limit ($h_\nu \ll M_e c^2$) of Compton scattering is the electronic Thomson scattering, so also the low-energy limit ($h_\nu \ll M_A c^2$) scattering of MeV photons by the nuclear point charge, is nuclear Thomson scattering. The corresponding scattering amplitudes are real, energy-independent, and are given by

$$a_{\parallel} = Z^2 e^2 / AM c^2, \quad (8a)$$

$$a_{\perp} = Z^2 e^2 \cos \theta / AM c^2. \quad (8b)$$

For unpolarized incident radiation the pure Thomson scattering cross section has the well-known form

$$\frac{d\sigma}{d\omega} = \frac{Z^4 e^4}{A^2 (M c^2)^2} \left(\frac{1 + \cos^2 \theta}{2} \right). \quad (9)$$

The Thomson amplitudes are of the same order of magnitude as the nuclear resonance amplitudes in medium and heavy nuclei for photon energies of about 10 MeV, and together these dominate the elastic scattering cross section at those angles where the Delbrück effect is small.

Delbrück scattering

Delbrück scattering can be viewed as a radiative correction to the nuclear Thomson scattering¹⁶ described above. The radiative corrections to this low-energy limit of Compton scattering describe the successive creation and annihilation of a real or virtual position-electron pair in the nuclear Coulomb field (Fig. 3); the energy of the incident and annihilated quanta being identical, this process, first predicted by Delbrück in 1932,¹ contributes to the elastic scattering amplitude. Furthermore, since the intermediate pair can be real or virtual, the scattering amplitude is complex; the real and imaginary parts corresponding to creation of virtual and real pairs, respectively.

The imaginary amplitudes at zero scattering angle can be obtained from the pair-production cross section via the "optical" theorem [Eq. (5)] and then the real part, the "vacuum polarization" term, is calculated for the zero scattering angle from the pair-production cross section by the dispersion relation [Eq. (4a)]. A direct confirmation of the existence of the real part of the Delbrück scattering amplitude would thus be an independent confirmation of the vacuum polarization. The earliest calculations of the Delbrück scattering amplitudes and cross sections were made in 1937. Bosch *et al.* have comprehensively reviewed all theoretical studies through 1962,⁴ most of these being for small scattering angles. One of the most important of these is the work of Kessler¹⁷ who calculated the imaginary scattering amplitude for arbitrary scattering angles and photon energies by a generalization of the optical theorem. He gives the imaginary Delbrück scattering amplitudes b_{\parallel}^D and b_{\perp}^D for each photon polarization in the form of a fivefold integral in which the integrand is the pair-production cross section $\sigma(\vec{k}, \vec{r})$; this must be evaluated numerically.

Ehlotsky and Sheppy¹⁸ have carried out this numerical evaluation of the imaginary amplitude for both photon polarizations over a large range of angles ($0 \leq \theta \leq 120^\circ$) and photon energies (1.3 MeV $\leq E_\gamma \leq 17$ MeV). They have used the property of analytic continuation to also evaluate the real amplitudes a_{\parallel}^D and a_{\perp}^D . From the Monte Carlo techniques used they estimate the accuracy of the calculated amplitudes. Generally these are about 90% accurate which gives an uncertainty of about 20% in the pure Delbrück cross section. These amplitudes are strongly forward peaked. Recently Mork and Papatzacos¹⁹ have also computed theoretical Delbrück scattering amplitudes for 10.83-MeV photons. At angles greater than 10° the imaginary amplitudes agree with those of Ehlotsky

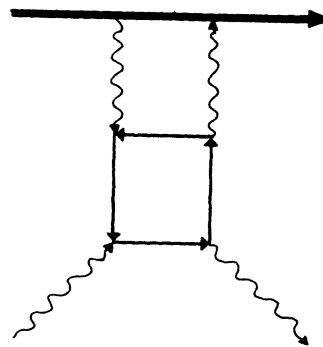


FIG. 3. Feynman diagram of the Delbrück scattering process showing the conversion of the incident photon to an electron-positron pair in the nuclear Coulomb field; the annihilation of this pair, real or virtual, generates the scattered photon.

and Sheppy but there is disagreement between the real amplitudes at all angles, these being not only opposite in sign but also about 40% smaller than those of Ehlotsky and Sheppy.

Ehlotsky and Sheppy have calculated the scattering amplitudes for photons of 9.00 and 13.29 MeV; for the values at 10.83 MeV a linear interpolation was used. If their Delbrück amplitudes are included at 120° the theoretical scattering cross section of uranium at 10.83 MeV is about 6% larger than for nuclear resonance and Thomson scattering alone. At 90° the cross section is predicted to be about 0.5% smaller if the Delbrück effect is included. A similar comparison at 90° using the Delbrück amplitudes of Mork and Papatzacos shows a reduction of about 5% when Delbrück scattering is included. Although we shall present evidence below to indicate that further calculations of Delbrück amplitudes are warranted, especially at intermediate and large angles, we have nonetheless assumed $a^D = b^D = 0$ for $\theta > 120^\circ$, specifically in evaluating the 150° measurements. In view of the angular variation of a^D this seemed a more cautious approach than to attempt an extrapolation to larger angles.

Nuclear resonance scattering

It is firmly established that below about 15 MeV in medium and heavy nuclei the photoabsorption cross section is dominated by $E1$ absorption to the giant dipole resonance. The damped harmonic-oscillator model offers a convenient parametrization of the process. In this picture the energy dependence of the absorption cross section is given as the sum of one or more Lorentzian-shaped resonances of the form

$$\sigma^{\text{abs}}(E) = \sigma_0 E^2 \Gamma / [(E_0^2 - E^2)^2 + E^2 \Gamma^2], \quad (10)$$

where the parameters E_0 , σ_0 , and Γ describe the energy, peak absorption cross section, and damping width, respectively. An empirical rule for the location of the state is $E_0 = 80A^{-1/3}$ MeV. The width Γ is in the range 4 to 8 MeV. For $A \approx 200$ this indicates a centroid of the giant resonance near 13 MeV and the Lorentzian distribution implies considerable $E1$ strength as low as 10 or 11 MeV. Elastic and inelastic scattering can take place through the two-step process in which first the incident photon is absorbed exciting the giant dipole resonance. The subsequent radiative decay of the intermediate state generates the scattered photon. For a $J^\pi = 0^+$ target nucleus the spin sequence for elastic scattering will be $0^+ \rightarrow 1^- \rightarrow 0^+$, and for inelastic scattering will be $0^+ \rightarrow 1^- \rightarrow 2^+$ to the first excited state of the target. Each sequence will give rise to characteristic angular distribu-

tions for the scattered photons, and a comparison with the observed distribution is an important check on the validity of this qualitative picture.

Implicit in this formulation is the assumption that excitation of individual nuclear states at these photon energies ($h\nu \sim 10$ MeV) is not meaningful. This can be argued since in the region of the continuum of interest the widths Γ of individual levels are much greater than the mean level spacing D . Under such conditions the only local statistical effect expected for elastic or inelastic scattering to discrete final states is Erickson fluctuations²⁰ in the corresponding cross sections. Experimentally, the importance of these fluctuations is determined by the relative magnitudes of the energy spread of the incident photon beam $\Delta E\gamma$ and the coherence width Γ_{coh} characteristic of the compound nucleus under study. If $\Gamma_{\text{coh}} \ll \Delta E\gamma$, the fluctuations will be averaged out and the experimental data can be interpreted in terms of the average properties characteristic of the target at that excitation, namely, those of the giant dipole resonance. Unfortunately, no experimental information exists for Γ_{coh} in the nuclei involved in our measurements, and any theoretical calculation is very speculative. Eberhard and Richter²¹ have summarized the data available. Their results, which are restricted to the mass region $A \lesssim 120$ and considerably higher excitation energies, suggest that $\Gamma_{\text{coh}} \ll \Delta E\gamma$ for the targets of interest to us. Hence, the existence of individual states at high excitation is ignored in the discussion which follows and the intermediate nuclear configuration is viewed as a single short-lived collective state with a decay width appropriate to the giant-dipole-resonance state.

If the angular distribution is known, the elastic nuclear resonance scattering amplitude at all angles can be given in terms of the zero-degree values. Furthermore, when the total photon absorption cross section is known, the zero-degree scattering amplitudes follow from Eqs. (5) and (6). Thus any model or parametrization which accurately describes the photoabsorption cross section must also predict correctly the elastic nuclear-resonance-scattering cross section. For the case of a single Lorentzian fit to the total photoabsorption cross section a calculation of the zero-degree real and imaginary elastic scattering amplitudes from Eqs. (6), (7) and (10) gives

$$a^{\kappa}(E, \theta = 0) = \frac{\Gamma \sigma_0}{4\pi e^2 \hbar e} E^2 \frac{E^2 - E_0}{(E_0^2 - E^2)^2 + \Gamma^2 E^2}, \quad (11a)$$

$$b^{\kappa}(E, \theta = 0) = \frac{\sigma_0 E}{4\pi e^2 \hbar e} E^2 \frac{E^2 \Gamma^2}{(E_0^2 - E^2)^2 + E^2 \Gamma^2}. \quad (11b)$$

From these and the angular distribution, the ampli-

tudes for the two photon polarizations are determined. For the spin sequence $0^+ - 1^- - 0^+$ these are

$$a_{\parallel}^{\kappa}(E, \theta) = a^{\kappa}(E, \theta = 0) \cos \theta \quad (12a)$$

$$a_{\perp}^{\kappa}(E, \theta) = a^{\kappa}(E, \theta = 0). \quad (12b)$$

The inelastic scattering cross sections are a different matter. A more detailed picture of the reaction mechanism is necessary to predict these values.

A convenient way to discuss the reaction is to use the simple rotator model of Danos and Okamoto.²² In this hydrodynamic model of a deformed nucleus three possible dipole modes of vibration are assumed, corresponding to vibrations along three independent axes. In a spherical nucleus these three modes are degenerate and the photo-absorption cross section is described by a single Lorentzian. In a prolate deformed nucleus the giant dipole resonance splits into two peaks: a lower-energy peak which describes oscillation along the symmetry axis and a higher-energy peak describing the faster oscillations along the two axes perpendicular to the symmetry axis. These latter two modes are degenerate so that the total $E1$ absorption strength is divided 1:2 between the lower- and higher-energy modes; both peaks in the absorption cross section should be individually described by a Lorentzian curve and the requirement that the area of the upper resonance curve be twice that of the lower means simply

$$2E_1\Gamma_1 = E_u\Gamma_u. \quad (13)$$

The splitting of the resonance ($E_u - E_l$) is caused by the quadrupole moment of the ground state in this model. The component at lower energy is associated with transitions for which $\Delta K = 0$ and that at the higher energy with transitions for which $\Delta K = \pm 1$ where K is the usual projection of the nuclear angular momentum on the symmetry axis. In this model coupling of the giant dipole resonance to the low-lying vibrational modes of excitation is neglected and consequently inelastic scattering is predicted only to states in the ground-state rotational band. If we let $A \equiv a_l + ib_l$ and $B \equiv a_u + ib_u$ be the complex resonance scattering amplitudes associated with the lower and upper resonances, respectively, and define $T \equiv a$ as the real Thomson scattering amplitude, then the conventional form²³ for the Danos-Okamoto model is

$$\left. \frac{d\sigma}{d\omega} \right|_0 = \left| \frac{A+2B}{3} + T \right|^2 \left(\frac{1+\cos^2\theta}{2} \right), \quad (14a)$$

$$\left. \frac{d\sigma}{d\omega} \right|_2 = (I_0 K_0 20 |I_f K_0|^2 \left| \frac{2}{3}(A-B) \right|^2 \left(\frac{13+\cos^2\theta}{40} \right)). \quad (14b)$$

Here the quantum numbers are I_0 and K_0 for the target ground state and I_f for the final state; the incident and outgoing radiation is unpolarized. These cross sections describe scattering with 0 and 2 units of angular momentum transferred to the target, respectively. The scattering amplitudes A and B are determined from the resonance parameters for each Lorentzian by application of Eqs. (11), and from (14) it is seen that scalar and tensor scattering can be identified by their angular distributions, a simple matter for a spin-zero target where these correspond uniquely to elastic and to Raman scattering, respectively. An alternative method to identify the scalar and tensor scattering has been discussed by Arenhövel and Hayward.²⁴ The first measurements of this type, i.e., using polarized photons, have recently been carried out at 15.1-MeV energy by Hayward, Barber, and Sazama²⁵ for vibrational nuclei.

At the time that measurements reported here were begun, accurate information on the photo-absorption cross section in heavy nuclei was limited. Recently, however, Bergere and co-workers²⁶⁻²⁸ have reported a series of precise measurements for nuclei between $Z = 65$ (Tb) and $Z = 92$ (U). In these the analysis of the photo-absorption cross section is given in terms of the two-Lorentzian theory. We have attempted to measure the same targets in order to make an effective comparison of theory and experiment. The resonance parameters used for these nuclei are given in Table II.

The simple rotator model has undergone several refinements which allow a more complete set of predictions. The dynamic collective model (DCM)²⁹ is a more sophisticated treatment which retains the basic Goldhaber-Teller model for the dipole oscillation and the rotational modes of intrinsic nuclear motion, but also includes low-energy surface vibrational modes and introduces the coupling between the dipole oscillations and the rotational and surface vibrational degrees of freedom. The effect of this coupling is to remove the degeneracy in the upper Lorentzian component. Another pre-

TABLE II. Giant-dipole-resonance parameters for nuclei studied in this experiment.

Target nucleus	E_1 (MeV)	σ_1 (mb)	Γ_1 (MeV)	E_2 (MeV)	σ_2 (mb)	Γ_2 (MeV)	$\frac{\sigma_2\Gamma_2}{\sigma_1\Gamma_1}$	Ref.
²³⁸ U ₉₂	10.96	301	2.90	14.04	369	4.53	1.91	28
²³⁵ U ₉₂	10.85	365	2.45	14.1	447	4.0	2.00	33
²³² Th ₉₀	11.08	268	3.37	14.07	349	4.62	1.79	28
²⁰⁸ Pb ₈₂	13.42	640	4.05				...	27
¹⁸¹ Ta ₇₃	12.35	270	2.57	15.30	330	4.47	2.13	26
¹⁵⁹ Tb ₆₅	12.12	205	3.25	15.97	240	4.87	1.75	23

diction of the DCM is that inelastic scattering with $\Delta K = 1$ states in the higher-lying γ -vibrational band should occur; the detection of such lines would be a direct verification of the model. Using this model, Arenhövel³⁰ has calculated the scattering cross sections for several of the nuclei we have studied. His results will be discussed in Sec. V.

Rayleigh scattering

Uncertainty in the scattering amplitudes for Rayleigh scattering, i.e., elastic scattering by the atomic electrons, has been the principal difficulty in all elastic scattering measurements below 10 MeV. The situation has been summarized recently by Schumacher, Smed, and Borchert.⁸ The scattering amplitudes calculated by means of the form-factor approximation of Franz³¹ are accurate only at very low photon energies. Calculations at higher energies, 0.6–2.6 MeV, have been made by Brown and Mayers³² using second-order perturbation theory and the Dirac equation for the k -shell Rayleigh amplitudes. In general the amplitudes are smaller than the form-factor predictions. However, lack of precise estimates of the scattering amplitudes and phases for other electron shells make accurate calculation of the total Rayleigh amplitude impossible. In the absence of such information, detailed interpretation of elastic scattering cross sections has not been possible. However, the results of calculations⁸ using relativistic Hartree-Fock-Slater wave functions clearly indicate that the form-factor approximation overestimates the scattering amplitudes for momentum transfers corresponding to elastic scattering of photons with $E_\gamma \approx 10$ MeV at scattering angles of ≈ 20 – 30° .

In view of past difficulties in accounting for Rayleigh scattering, our measurements were planned for photon energies where calculated Rayleigh scattering amplitudes were at least an order of magnitude smaller than the nuclear resonance amplitudes. Estimates of the Rayleigh amplitudes were made by neglecting the imaginary part which is known to be small at these energies and approximating the real part by the value obtained from the form-factor approximation. Because this upper limit was always less than the uncertainty in the value of the scattering amplitude calculated for the other coherent processes, the Rayleigh amplitudes were neglected at 10.83 MeV.

To obtain the correct total differential elastic scattering cross section, the relative phases of the various amplitudes must be known. The observation of a characteristic interference minimum in the scattering cross section of heavy

nuclei below the giant dipole resonance indicates that the nuclear Thomson and nuclear resonance amplitudes are of opposite phase. Hardie, Merrow, and Schwandt¹⁰ have pointed out that dispersion relations can be used to establish the phases between the real part of the Delbrück and nuclear resonance amplitudes in the forward direction. The phases at other angles then can be determined from the calculated angular dependence. Similarly, the phases for the imaginary parts of the Delbrück and nuclear resonance amplitudes can be established by application of the optical theorem. In the forward direction the two polarization components must be identical and the phase choices outlined apply to either polarization state. Thus the real and imaginary parts of the total scattering amplitudes are given for each photon polarization by

$$a = a^D + a^K - a^T, \quad (15a)$$

$$b = b^D + b^K. \quad (15b)$$

IV. EXPERIMENTAL RESULTS

Angular distributions were measured for Pb and U. A portion of the U data has been shown in Fig. 2. For the other nuclei only the 90° scattering

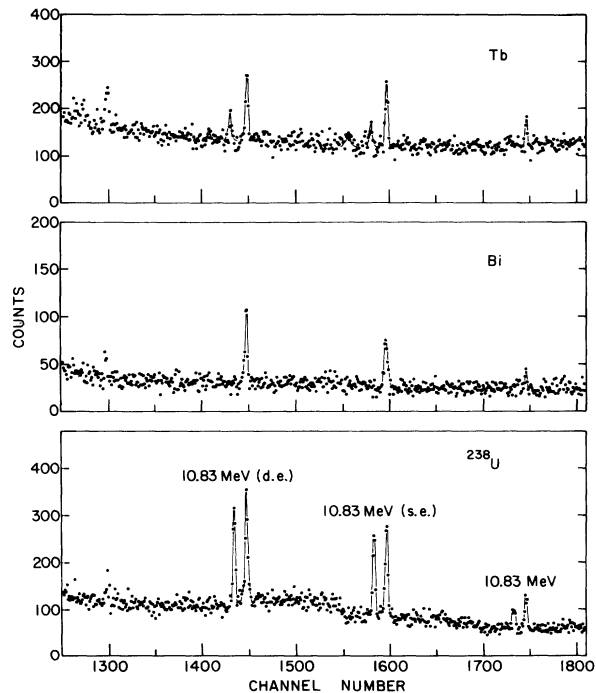


FIG. 4. High-energy portions of the spectra of 10.83-MeV radiation scattered from U, Bi, and Tb targets at 90° . The U spectrum is similar to that shown in Fig. 2 except that the spectrum was detected by a Ge(Li) system cooled with liquid A_2 , as were the Bi and Tb spectra.

was measured. These spectra for Bi and Tb, together with a U 90° spectrum in which liquid-argon coolant was used, are shown in Fig. 4. The cross sections for elastic and inelastic scattering obtained at each angle from these and similar spectra are tabulated in Table I for all the targets studied. Though the spectra were scanned for evidence of lines corresponding to scattering to other excited states, only members of the ground-state rotational bands were observed to be populated in these measurements for all deformed targets. Columns 2 and 3 of Table III compare the value $d\sigma(90^\circ)/d\omega$ for elastic scattering by each target calculated as outlined above with the value measured in this experiment. The agreement, with the exception of Ta, is very good. Because the relationship between these two types of data is model-independent, i.e., follows from very basic principles, this agreement increases our confidence in the absolute calibration of our experiment and indicates that the problems encountered in the measurement reported in Ref. 13 have been solved. It is particularly valuable to compute the ratio of the Raman to the elastic scattering, since it can be deduced directly from the relative intensities of the corresponding peaks in the scattered spectrum and is therefore free of any systematic errors in normalization. A tabulation of the measured and calculated values of this ratio at 90° is given in columns 4 and 5 of Table III. The calculation uses the appropriate parameters for the giant dipole resonance (Table II) in the Danos-Okamoto theory, Eqs. (12a) and (12b). Except for Tb, the predicted and measured ratios are within about 2 standard deviations; yet the experimental values are less than the calculated values in all cases. For Tb the measured value is much smaller. A discussion of the data

TABLE III. Comparison of calculated and observed values of the 90° cross sections for elastic scattering and of the ratio at 90° of Raman to elastic scattering by various nuclei for 10.83-MeV photons. The parameters used in the calculations are given in Table II.

Target	$d\sigma_{\text{elas}}(90^\circ)/d\Omega$ (mb/sr)		$d\sigma_{\text{Raman}}^{(90^\circ)}/d\sigma_{\text{elas}}^{(90^\circ)}$	
	Calc	Exp	Calc	Exp
Tb	0.036	0.031 ± 0.003	0.80	0.51 ± 0.06
Ta	0.055	0.037 ± 0.003	0.28	0.18 ± 0.04
Pb	0.076	0.079 ± 0.005	0	
Bi		0.101 ± 0.006	0	~ 0
Th	0.128	0.129 ± 0.015	0.91	0.80 ± 0.08
U	0.157 ^a	0.182 ± 0.017	1.03	0.85 ± 0.08

^a If the Livermore parameters (Ref. 33) for ^{235}U are used then this calculated value would be 0.210 mb/sr.

individually for each target which follows will facilitate interpretation of these results.

^{238}U

The cross sections observed for the elastic and the Raman scattering are shown in Fig. 5. The solid curves are the cross sections calculated using the scattering amplitudes discussed in Sec. 2. The cross section for elastic scattering includes contributions from Delbrück scattering using the amplitudes of Elotsky and Sheppy, from nuclear resonance scattering using the parameters for the giant dipole resonance deduced by Bergere *et al.*, and from nuclear Thomson scattering. Since only the latter two processes should contribute appreciably to the cross section in the back hemisphere, the angular variation predicted from Eqs. (8) and (12a) is $(1 + \cos^2\theta)$. Reflection

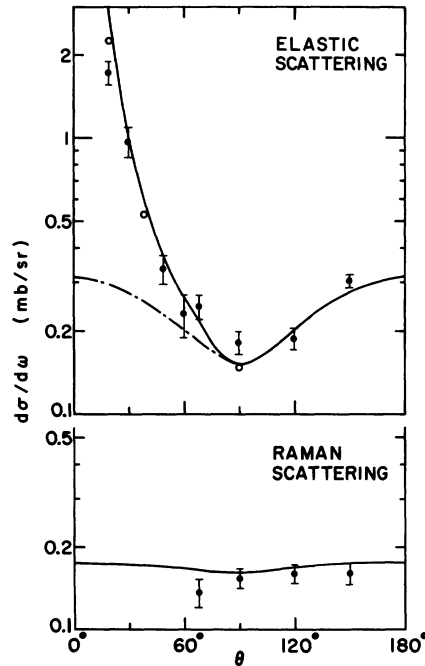


FIG. 5. Angular variation of the elastic and Raman scattering cross sections for uranium at 10.83 MeV. The measured values are shown together with the statistical errors of measurement. The solid curve in each case represents the calculated values. For elastic scattering the broken curve shows the calculated values in the forward direction when Delbrück scattering is neglected. The Delbrück amplitudes of the CERN group (Ref. 18) are used to compute the solid curve; those of the Trondheim group (Ref. 19) give similar values. These are indicated by the open circles at 20° , 50° , and 90° , but at 30° and 70° the two sets of values are so close as to be indistinguishable in the figure. The solid curve in the lower portion of the figure is the prediction of the simple rotator model discussed in the text.

of this curve into the forward hemisphere (shown by the dashed curve) gives the cross section expected in the absence of Delbrück scattering. As the data indicate, the measured differential cross section at forward angles is much larger than that calculated with no Delbrück amplitude and this difference has been interpreted as an unambiguous observation of the Delbrück effect.

As noted in Sec. 2, there is a major discrepancy between predictions reported for the real part of the Delbrück amplitudes. The circles of Fig. 5 indicate cross sections calculated using the Delbrück amplitudes of Mork and Papatzacos. At 20° these are $\sim 20\%$ lower than the Ehlotsky and Sheppy values. In view of this uncertainty in the theory and the possible contribution of Rayleigh scattering, any significance in the discrepancy between the measured and predicted values at the forward angles should be minimized. For $\theta \geq 30^\circ$ the two theories yield similar results for uranium, and the agreement between measured and calculated cross sections is good.

The measured cross section for Raman scattering to the 45-keV state is compared to the predictions of the Danos-Okamoto simple rotator model using the parameters of Bergere *et al.* in the lower part of Fig. 5. The model values obtained from Eqs. (14) are shown as the solid curve. The measured cross sections agree well with the angular distributions of Eqs. (14), indicating that the assumption of an intermediate state with $J^\pi = 1^-$ is valid.

The ratio of the Raman to the elastic cross section can be determined directly from the scattered spectrum with a precision considerably higher than the errors as the individual cross sections would indicate. For U at 90° this ratio is 0.85 ± 0.08 , whereas the value of 1.03 is predicted by the Danos-Okamoto theory. Arenhövel has calculated this ratio on the basis of the dynamic collective model and has obtained a similar result. At 150° the ratio is 0.53 ± 0.05 compared with a prediction of 0.62. Thus it is unlikely that the discrepancy can be attributed to a residual contribution from the Delbrück effect. The data suggest that the Raman scattering is weaker than predicted.

At the time of the preliminary report of our results in Ref. 13 giant-dipole parameters for ^{238}U were not available. Because no significant isotopic dependence was expected for the giant dipole resonance in U, the ^{238}U data were analyzed in terms of photoabsorption parameters for ^{235}U . However, the giant-dipole parameters reported³³ for ^{235}U and ^{238}U have recently been shown to differ. Use of the ^{238}U parameters in place of those for ^{235}U to calculate the elastic and inelastic scatter-

ing cross sections decreases the elastic cross section by 35% and gives a Raman to elastic ratio of 1.03 in place of 1.3. The apparent agreement reported in Ref. 13 between our observed $d\sigma(90^\circ)/d\Omega$ and the value implied by the ^{235}U data is destroyed by the improved absolute normalization discussed above. For $\theta \geq 90^\circ$ both the value of the elastic cross section and the Raman to elastic ratio are in better agreement with the most recent data from Saclay for ^{238}U .

^{232}Th

Observations were extended to a second deformed actinide target with measurements at 90° of scattered spectrum for ^{232}Th . For elastic scattering, $d\sigma(90^\circ)/d\Omega = 0.129 \pm 0.015$ mb/sr is measured. The value 0.128 mb/sr is predicted by the simple rotator model using the parameters given in Table II. Again the good agreement confirms the internal consistency of the absolute normalizations of our two sets of measurement experiments. The level scheme for ^{232}Th is similar to that of ^{238}U with an identical spin sequence for the low-lying levels. Because the quadrupole moments of ^{232}Th and ^{238}U are almost the same, 9.66 and 11.3 b, respectively,³⁴ the level spacings are also similar. In this target the Raman scattering excites the 49.8-keV first excited state whose $J^\pi = 2^+$. The experimental value of the Raman to elastic scattering is 0.80 ± 0.08 compared with the simple-rotator-model prediction of 0.91. Again this ratio is about 10% less than the predicted value, although in this case the discrepancy is not statistically significant.

^{209}Bi

The spherical nucleus ^{209}Bi was studied in order to establish an upper limit on inelastic scattering expected in the absence of rotational coupling between the giant dipole resonance and low-lying states. The first excited state of ^{209}Bi at 910 keV ($J^\pi = \frac{7}{2}^-$) can be interpreted as a simple $2f_{7/2}$ single-particle proton excitation. Although excitation of this level by Raman scattering is allowed on the basis of angular momentum consideration, no coupling to low-lying particle excitations exists in the single hydrodynamic model and the cross section of inelastic scattering corresponding to this residual state should vanish. The data are consistent with this. The experimental ratio of Raman scattering to elastic scattering is ≤ 0.1 . Unfortunately, no reliable parameters exist for the giant dipole resonance in Bi, although the measurements of Harvey *et al.*³⁵ suggest that the peak photoabsorption cross section in Bi may be 5% higher than ^{208}Pb . Because the elastic scat-

tering cross is proportional to the square of the absorption cross section, such uncertainties are doubled. For this reason a precise prediction for the 90° elastic scattering cross section is not available for comparison with the experimental value of 0.101 ± 0.006 .

Pb

The main interest in the Pb measurements was the elastic scattering. A natural target was used. The only isotope with a nonzero ground-state spin is the 23% abundant ^{207}Pb , $J^\pi = \frac{1}{2}^+$. It can be readily shown from Eqs. (14) that only scalar scattering contributes to the elastic cross section for such a state. Thus for our purposes Pb can be considered as a target with $J^\pi = 0^+$. In Fig. 6 the experimental data are given together with several calculated elastic scattering cross sections. As for U, the scattering for $\theta \leq 60^\circ$ is much stronger than scattering in the back hemisphere indicating the dominance of the Delbrück effect at forward angles. At 90 and 150° the results are in good agreement with the values which follow from the photoabsorption data for ^{208}Pb , i.e., with no Delbrück contribution. At other angles, discrepancies between prediction and experiment are apparent from the figure. There are two possible sources for this. First, as seen in Fig. 6, a sizable difference results when the cross sections calculated with the Delbrück amplitudes of the CERN group¹⁸ are compared with those calculated with the corresponding amplitudes of the Trondheim¹⁹ group which has computed amplitudes for $\theta \leq 90^\circ$. However, because both calculations are less than the measurements for $\theta = 50$ and 60° while the use of the CERN amplitudes clearly overestimate the 120° cross section, it is unlikely that the discrepancies can be attributed solely to inaccurate Delbrück amplitudes.

Recently, Lewis, Bertrand, and Horen³⁶ and Buskirk *et al.*³⁷ have reported evidence for an $E2$ resonance in ^{208}Pb at 10.8 MeV. Since the $E2$ resonance is much weaker than the giant dipole resonance, the main effect of such a mode of absorption on the elastic photon scattering will be to introduce an interference term into the angular distribution. It can be readily shown that this term is $Q \cos\theta$, i.e., the interference is antisymmetric about 90° as is required for interference between waves of opposite parity. Such an effect is qualitatively similar to the trend of the deviations from the curves of Fig. 6 near 60 and 120° . However, in the absence of accurate parameters for the $E2$ resonance and also in view of the uncertainties in the Delbrück amplitudes no quantitative conclusions can be drawn. Thus, we can only conclude that the data are consistent with

a weak interference term characteristic of interference between scattering by $E2$ and $E1$ giant dipole states.

^{159}Tb and ^{181}Ta

Tb and Ta are strongly deformed nuclei in the rare-earth region. For $A = 160$, the location of the giant dipole state is predicted to be $E_0 \approx 14.7$ MeV, but as a result of the large quadrupole moments of these targets the giant dipole resonance is split and a sufficient $E1$ strength is lowered to energies of ~ 10 MeV to produce sizable resonance scattering of photons. Because both targets have ground-state spins greater than $\frac{1}{2}$, tensor scattering can contribute to the elastic scattering. According to the simple rotator model [Eqs. (14)] the tensor contribution to resonance scattering exciting the $\frac{7}{2}^-$, $\frac{9}{2}^-$, and $\frac{11}{2}^-$ members of the ground-state rotational band of Ta are in the proportions $-5:4:1$. The corresponding ratios for the $\frac{3}{2}^+$, $\frac{5}{2}^+$, and $\frac{7}{2}^+$ members of the ground-state rotational band of Tb are $2:5:3$, respectively. In both nuclides, scalar scattering also contributes to the elastic scattering. The parameters used for these calculations are given in Table II.

For Ta only scattering to the ground state and first excited states were observed, but in view of the predicted intensity of scattering to the $\frac{11}{2}^-$ level, no significance can be given to the absence of this Raman line. Both elastic and Raman scattering are significantly weaker than expected on the basis of the simple rotator model (see Table

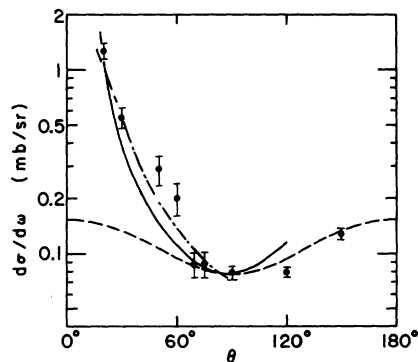


FIG. 6. Angular variation of the elastic scattering cross section in lead. The measured values are shown together with the errors of measurement. The solid curve represents the values calculated using the Delbrück amplitudes of the CERN group (Ref. 18), the broken curve, using those of the Trondheim group (Ref. 19), and the dashed curve is the variation expected for no Delbrück scattering. The two curves which include Delbrück scattering are extended only to the same large angle for which the corresponding Delbrück amplitudes have been computed.

III) and the ratio of the Raman to elastic scattering is much less than the predicted value.

For the Tb target scattering to all three members of the ground-state band was detected. The elastic scattering cross section at 90° is in fair agreement with the calculated value, but again the Raman component is significantly weaker than expected. As Table III indicates, the Raman to elastic ratio is again less than the simple rotator model.

V. SUMMARY

The results of the measurements reported here are summarized in the following conclusions: (1) Elastic scattering in high- Z targets for forward scattering angles is dominated by the Delbrück effect; (2) for $\theta \geq 90^\circ$, where only the nuclear resonance and Thomson scattering are important, both the magnitude and the angular dependence of the elastic scattering cross section are in substantial agreement with the values which follow from the most recent photoabsorption cross sections in the corresponding targets, with the possible exception of Ta; (3) a systematic trend of Raman scattering to be weaker by 10% or more than expected is suggested by the data for U, Th, Ta, and Tb. Points 1 and 3 require further comment.

The computations of Ehlotsky and Sheppy indicate that the real and imaginary parts of the Delbrück amplitudes are comparable in size at those scattering angles for which the Delbrück effect is evident in our data. As calculated by them the signs are such that the imaginary part b^D interferes constructively with the imaginary nuclear amplitude b^K , while the real part a^D interferes destructively with the net real nuclear amplitude ($a^K - a^T$). Moreover, because the magnitude of a^D is comparable to ($a^K - a^T$) in these heavy nuclei, U and Pb, the major contribution to the calculated elastic scattering cross section comes from the imaginary Delbrück amplitudes. Thus the calculation based on the work of Ehlotsky and Sheppy is not sensitive to the presence or absence of a real amplitude. In U and Pb it is only at the extreme forward angles $\theta \leq 20^\circ$ that the contribution of the real amplitude becomes significant. This is the region where the onset of Rayleigh scattering should occur and obscure any analysis or interpretation of data. Thus the agreement in U (Fig. 5) between the calculated and observed values of the elastic scattering at the forward angles $\theta > 20^\circ$ confirms only the imaginary Delbrück amplitudes of Ehlotsky and Sheppy. No conclusions can be drawn about the real amplitudes.

Because real Delbrück amplitudes computed by

Mork and Papatzacos have the same sign as the net real nuclear amplitude ($a^K - a^T$) they would predict a contribution from both the real and the imaginary amplitudes, albeit the imaginary amplitudes are larger. As discussed for Fig. 6 these calculated values for U do not differ markedly from the other calculations. For Pb the Mork and Papatzacos amplitudes predict a somewhat higher cross section for the intermediate angles $30^\circ \leq \theta \leq 70^\circ$. However, because of a possible enhancement from an $E2$ interference discussed above one cannot conclude that there is better agreement in Pb solely as a result of choosing another set of Delbrück amplitudes. In short neither the U nor the Pb elastic scattering measurements reported here permit one to draw any conclusions about the real Delbrück amplitude.

With regard to point 3 above, in comparing the data for scattering into the back hemisphere with the predictions of the simple rotator model it should be emphasized that the error in the absolute normalization, $\sim 8\%$, is a systematic error in its effect on the data points. Thus, the hypothesis³⁰ that the $\sim 10\%$ discrepancy in the relative strengths of elastic and Raman scattering observed for U and Th is due to a deviation of one or the other from the prediction of the simple rotator model cannot be tested by comparing the absolute cross sections with prediction. It is for this reason that our discussion has focused on the ratio of the Raman to elastic scattering and its comparison with the corresponding simple-rotator-model value.

In the simple-rotator theory the radial parts of the matrix elements associated with transitions between the giant dipole resonance and all members of the ground-state rotational band are the same. The relative intensities of all the lines in the ground-state band will be given by the angular momentum factors indicated in Eqs. (14), which lead to the calculated values for the ratio of the Raman to elastic strength tabulated in column 4, Table III. These estimates are systematically larger than the measured ratios as this tabulation indicates. The tendency of the simple model to overestimate this ratio could be explained if the deformed targets were not good rotators. In this case the theoretical ratios would be less than the values tabulated. However, since the low-lying levels of these targets accurately follow the spin and spacing sequence characteristic of the rotational collective model, this explanation seems very improbable. Arenhövel³⁸ has explored the possibility of a more likely explanation—the presence of a substantial direct or nonresonant reaction component in the region of the giant dipole resonance. The major conclusion of his

treatment is that a nonresonant reaction strength which varies slowly with energy will result in yet another scattering amplitude which is pure imaginary. Because this reaction is assumed to be independent of nuclear orientation, the corresponding amplitude will contribute to the scalar but not the tensor scattering amplitudes. Thus for a spin-0 target, the nonresonant reaction should contribute only to the elastic scattering and therefore depress the Raman to elastic ratio. Using the same notation as before for A and B of Eqs. (14), Arenhövel shows that at 90° in the absence of Delbrück scattering the ratio of tensor to scalar scattering (which for a spin-0 target is the same as the Raman to elastic ratio) is

$$R \equiv \frac{d\sigma_{2+}}{d\sigma_{0+}} = \frac{13(a_i^K - a_u^K)^2 + (b_i^K - b_u^K)^2}{5(a_i^K + 2a_u^K - 3Z)^2 + (b_i^K + 2b_u^K)^2(1 + \epsilon)^2}, \quad (16)$$

where Z is the Thomson scattering amplitude in units of $(NZ/A)(e^2/Mc^2)\beta$ and ϵ is the ratio of the nonresonant to the resonant imaginary amplitude, assumed to be the same for the lower and the upper resonance.

Evidence for nonresonant processes comes from experiments^{39, 40} in which the nuclear absorption of photons by aligned ¹⁶⁵Ho targets was studied. The data show a larger ratio of scalar to tensor polarizability than expected. This scalar enhancement has been attributed to direct processes. A direct-reaction component accounting for 10–20% of the absorption cross section would explain the observed ratio. Thus, it would be surprising if the photon scattering cross sections did not show a tendency toward values of R somewhat below the predicted value. Our results for U and Th can be explained by including a relatively small, ~5%

direct amplitude, $\epsilon \approx 0.05$, in Eq. (16). The results for Tb and Ta are consistent with direct amplitudes in the range 10–20%, that is $\epsilon \approx 0.1$ to 0.2, which is consistent with the photoabsorption results for Ho.

Preliminary data have been reported at 11.38 MeV by Bar-Noy and Moreh⁴¹ who observe a value for R at 140° in U of 0.80 ± 0.14 , which is consistent with their calculated value of 0.83. From this single measurement the errors do not allow one to confirm or deny the trend of a diminished Raman to elastic ratio at this photon energy. A confirmation of this trend in R could again be made by a sequence of measurements over a range of targets.

It is evident from the data presented here that measurements covering deformed nuclei in the actinide and lanthanide regions and spanning a range of photon energies in the region of the giant dipole resonances would yield information of great value in understanding the photonuclear interaction.

ACKNOWLEDGMENTS

The authors wish to express their gratitude to H. Arenhövel for his continuing interest and suggestions for interpretations of the data, to F. Coester and F. Ehlotsky for clarifying several aspects of the theory and analysis of earlier experiments. We are particularly indebted to K. Mork and P. Papatzacos for furnishing results of their Delbrück calculations prior to publication. We wish to thank E. Hayward for her encouragement, and G. Hardie for his comments. The technical assistance of J. Specht was invaluable to the completion of the experiments.

*Work performed under the auspices of the U. S. Atomic Energy Commission.

¹M. Delbrück, *Z. Phys.* **84**, 144 (1933).

²Z. Maric and P. Móbrus, *Nucl. Phys.* **10**, 135 (1958).

³U. Fano, *On the Scattering of γ Rays by Nuclei*, National Bureau of Standards Technical Note No. 83 (U.S. GPO, Washington, D. C., 1960).

⁴For a review of early work, see R. Bösch, J. Lang, R. Müller, and W. Wölfi, *Helv. Phys. Acta* **36**, 625 (1963).

⁵R. Bösch, J. Lang, R. Müller, and W. Wölfi, *Phys. Lett.* **2**, 16 (1962) and Ref. 3.

⁶H. E. Jackson and K. J. Wetzel, *Phys. Rev. Lett.* **22**, 1008 (1969).

⁷R. Moreh, D. Salzman, and G. Ben-David, *Phys. Lett.* **34B**, 494 (1971).

⁸M. Schumacher, F. Smend, and I. Borchert, *Nucl. Phys.* **A206**, 531 (1973).

⁹G. Basavarju and P. P. Kane, *Nucl. Phys.* **A149**, 49 (1970).

¹⁰G. Hardie, W. J. Merrow, and D. R. Schwandt, *Phys. Rev. C* **1**, 714 (1970).

¹¹E. Hayward, *Photonuclear Reactions*, National Bureau of Standards Monograph No. 118 (U.S. GPO, Washington, D. C., 1970), p. 70.

¹²E. G. Fuller and E. Hayward, *Nucl. Phys.* **30**, 613 (1962).

¹³K. J. Wetzel and H. E. Jackson, *Bull. Am. Phys. Soc.* **16**, S79 (1971); H. E. Jackson and K. J. Wetzel, *Phys. Rev. Lett.* **28**, 513 (1972).

¹⁴M. Hass, R. Moreh, and D. Salzman, *Phys. Lett.* **36B**, 68 (1971).

¹⁵See the discussion of J. J. Sakurai, *Advanced Quantum Mechanics* (Addison-Wesley, Reading, Mass., 1967), p. 57.

¹⁶J. N. Jauch and F. Rohrlich, *The Theory of Photons*

- and Electrons* (Addison-Wesley, Reading, Mass., 1955), p. 379.
- ¹⁷P. Kessler, *J. Phys. (Paris)* **19**, 739 (1958).
- ¹⁸F. Ehlotzky and G. C. Sheppy, *Nuovo Cimento* **33**, 1185 (1964).
- ¹⁹K. Mork and P. Papatzacos, private communication.
- ²⁰T. Ericson and T. Mayer-Kuckuk, *Annu. Rev. Nucl. Sci.* **16**, 183 (1966).
- ²¹K. A. Eberhard and A. Richter, in *Statistical Properties of Nuclei*, edited by J. B. Garg (Plenum, New York, N. Y., 1972), p. 139.
- ²²M. Danos, *Nucl. Phys.* **5**, 23 (1958).
- ²³Reference 11, p. 9.
- ²⁴H. Arenhövel and E. Hayward, *Phys. Rev.* **165**, 1170 (1968).
- ²⁵E. Hayward, W. C. Barber, and F. Sazama, *Phys. Rev. C* **8**, 1065 (1973).
- ²⁶R. Bergère, H. Beil, and A. Veyssiere, *Nucl. Phys. A* **121**, 463 (1968).
- ²⁷A. Veyssiere, H. Beil, R. Bergère, P. Carlos, and A. Lepretre, *Nucl. Phys. A* **159**, 561 (1970).
- ²⁸A. Veyssiere, H. Beil, R. Bergère, P. Carlos, and A. Lepretre, *Nucl. Phys. A* **199**, 45 (1973).
- ²⁹M. Danos and W. Greiner, *Phys. Rev.* **134**, B284 (1964).
- ³⁰H. Arenhövel, Lawrence Livermore Laboratory Report No. CONF-730301, 1973 (unpublished), p. 449.
- ³¹W. Franz, *Z. Phys.* **98**, 314 (1936).
- ³²G. E. Brown and D. F. Mayers, *Proc. Roy. Soc. A* **242**, 89 (1957).
- ³³C. D. Bowman, G. F. Auchampaugh, and S. C. Fultz, *Phys. Rev.* **133**, B676 (1964).
- ³⁴K. E. G. Löbner, M. Vetter, and V. Hönig, *Nucl. Data* **7**, 5 (1970).
- ³⁵R. R. Harvey, J. T. Caldwell, R. L. Bramblett, S. C. Fultz, *Phys. Rev.* **136**, B126 (1964).
- ³⁶M. B. Lewis, F. E. Bertrand, and D. J. Horen, *Phys. Rev. C* **8**, 398 (1973).
- ³⁷F. R. Buskirk, H. D. Gräf, R. Pitthan, H. Theissen, O. Titze, and T. Walcher, *Phys. Lett.* **42B**, 194 (1972).
- ³⁸H. Arenhövel, *Phys. Rev. C* **6**, 1449 (1972).
- ³⁹E. Ambler, E. G. Fuller, and H. Marshak, *Phys. Rev.* **138**, B117 (1965).
- ⁴⁰M. A. Kelly, B. L. Berman, R. L. Bramblett, and S. C. Fultz, *Phys. Rev.* **179**, 1194 (1969).
- ⁴¹T. Bar-Noy and R. Moreh, *Ref.* **30**, p. 319.